

# Significant Role of Fe<sup>3+</sup> Sites on the Activation Energy Barrier at Electrode Interface in SnO<sub>2</sub>-Fe<sub>2</sub>O<sub>3</sub> Composite Based Hydroelectric Cell

Abha Shukla<sup>\*1,2</sup>, Sunidhi Badola<sup>1,2</sup> and Jyoti Shah<sup>1</sup>

<sup>1</sup>CSIR-National Physical Laboratory, Dr. K S Krishnan Road, Delhi-110012, India

<sup>2</sup>Academy of Scientific and Innovative Research (AcSIR), Ghaziabad, Uttar Pradesh, 201002, India

\*Corresponding Author : [abha2shukla@gmail.com](mailto:abha2shukla@gmail.com)

**Abstract:** Hydroelectric cell (HEC) is a green energy device known for its potential to replace solar cell and fuel cell in coming decades. Among number of materials explored, tin oxide-based cells have shown a huge potential to deliver high current densities with high activation losses. In this study, to overcome the activation loss, tin oxide-hematite composite based HEC power characteristics has been analysed. The composite cell delivered a short circuit current density of  $I_{sc} \sim 7.0$  mA/cm<sup>2</sup> and peak power of  $P_{den} \sim 26.9$  mW. More structural defects were found to nucleate in the composite compared to pure tin oxide confirmed by X-ray diffraction (XRD) and Raman spectroscopy. Scanning electron microscopy (SEM) revealed the high surface area and porous microstructure of the composite. Fourier transform infrared spectroscopy (FTIR) confirmed the presence of chemi-dissociated and physisorbed water molecules on the composite surface. The composite based hydroelectric cell displayed low activation losses compared to the bare SnO<sub>2</sub> HEC observed by the V-I characteristics. A significant role of Fe<sup>3+</sup> cations has been found crucial for the reduction in activation energy barrier in the composite based HEC.

**Keywords:** Tin Oxide, Hematite, HEC, Water splitting, Activation energy

**1. Introduction:** Energy generation in a sustainable way is the foremost requirement in today's scenario. As the global concern has risen towards the environmental crisis, it has become more important to generate energy in the greener way. Hydroelectric cell (HEC) is one of such energy sources known to generate electricity and hydrogen without polluting the environment [1,2]. Till date, a number of materials have been successfully synthesized to fabricate hydroelectric cell and among all tin oxide-based cells have shown promising results [3-7]. The primary requirement for the cell material is its oxygen deficient, nanoporous structure. The reaction in hydroelectric cell is initiated by the interaction of water molecules with the defective material surface followed by its chemisorption and then physi-dissociation. Defects mediated catalytic reactions on semiconducting oxide's surface has attracted the world-wide attention due to fast rate of reaction. Catalysts initiate a wide variety of energy extensive reactions at low energy potentials by providing an alternative

route with low energy barrier [8-10]. Water splitting is also an energy intensive process, on high energy defective material surface. Water splits by forming bond with the two neighboring defect sites (under coordinated cation and oxygen vacancy) and restructuring the material surface to low energy, the process known as the chemi-dissociation of water [11]. Splitting of physisorbed water in hydroelectric cell takes place via high electric potential created by the accumulation of charges (hydronium ions) inside nanopores [1]. The transfer/migration of these ions from the material surface to respective electrode is a crucial process. The supply and accumulation of ions determines the rate of reaction at the electrode and consequently the power output of the HEC. In tin oxide, water dissociation takes place in abundance due to inherent defects and the material exhibits high activation losses due to changes in its chemistry on interaction with water. Consequently, it affects the reactions at electrode and hence the polarization losses.

Although the internal resistance of tin oxide is low in comparison to other materials like silica, alumina, magnesium oxide etc. which shows high charge transfer resistance due to resistive grain boundaries [3]. This charge transfer resistance was found to decrease by multiple orders in antimony doped tin oxide (Sb-SnO<sub>2</sub>) which resulted into high currents and low activation and ohmic polarizations [7]. However, in Sb-SnO<sub>2</sub> the transformation of material take place which limits its durability for long. On the other hand, iron oxides are abundant, low cost and eco-friendly materials. Various iron oxides have been used for hydroelectric cell application. From the iron oxides based hydroelectric cells it was conclusively found that magnetite (Fe<sub>3</sub>O<sub>4</sub>) showed highest current density with low open circuit potential (OCP) and high activation losses due to the oxidation of Fe<sup>2+</sup> ions as the case in SnO<sub>2</sub> [6]. Maghemite ( $\gamma$ -Fe<sub>2</sub>O<sub>3</sub>) showed low current owing to the cation vacancies in the material which led to the associative adsorption of water at material surface [12]. Amongst all hematite ( $\alpha$ -Fe<sub>2</sub>O<sub>3</sub>) showed the maximum OCP of 0.92 V and short circuit current of 30 mA with the least activation losses owing to low energy barrier in the fabricated cell [13]. Therefore, in this study, hematite was used to synthesize a composite with tin oxide. The engineering of tin oxide to alter H<sub>2</sub>O-SnO<sub>2</sub> interaction chemistry for the tuning of polarization losses can make it a better alternative amongst all materials.

**2. Material and methods:** SnO<sub>2</sub>-Fe<sub>2</sub>O<sub>3</sub> composite was synthesized by solid state reaction. Analytical grade precursors- SnO<sub>2</sub> (Thomas Baker, 99% pure) and Fe<sub>2</sub>O<sub>3</sub> (Alfa-Aesar 99.9 % pure) were used without further purification. SnO<sub>2</sub> and Fe<sub>2</sub>O<sub>3</sub> taken in stoichiometric molar ratio 0.8:0.2 were wet grinded using acetone in pestle mortar for 1 hour. Sample was pre-sintered at 750 °C for 2 hours. Mixture was further hand grinded and pelletized using a manual hydraulic press into a 2 × 2 × 0.1 cm<sup>3</sup> pellet followed by sintering at 950 °C for 3 hours. The pure SnO<sub>2</sub> sample was also processed in the similar way. Hydroelectric cell was fabricated with both the pellets by pasting zinc anodic sheet on one face

and silver paste on the other face. Electrical contact wires were taken from individual electrodes to test the performance of SnO<sub>2</sub>-Fe<sub>2</sub>O<sub>3</sub> composite hydroelectric cell. X-ray diffraction (XRD) analysis of the pure and composite samples was performed with Bruker AXS D8 advance XRD, Cu-K $\alpha$  radiation of wavelength  $\lambda$ = 1.542 Å to investigate the phase of the samples. Scanning electron microscopy (Bruker AXS Microanalysis GmbH, Germany) and energy dispersive X-ray spectra (EDX) of the sample was obtained to analyze the surface morphology and elemental composition of the sample respectively.

Raman spectroscopy using the laser excitation wavelength of 514.5 nm was performed by Renishaw in-Via Raman spectrometer to examine the micro structural disorders in the samples before and after making the composite. Photoluminescence spectroscopy was performed with Perkin Elmer LS55 luminescence spectrometer to detect the formation of defect levels within the band gap of pure and composite samples. Characteristic V-I polarization curve was plotted by varying external loads using a Keithley power source meter to investigate the performance of the composite based HEC cell with respect to pure tin oxide based HEC. Sn-O, Fe-O and hydroxyl groups on the sample surface were characterized by PerkinElmer 1750 FTIR spectrophotometer. Electrochemical impedance spectroscopy of the pure and composite based wet HEC was performed using Wayne-Kerr Impedance Analyzer 6500B (UK) at an applied AC voltage of 10 mV in the frequency range 20-200MHz.

**3. Results and Discussion:** Composite samples have been analyzed by its X-ray diffraction pattern shown in Figure 1. Distinct polycrystalline XRD peaks attributing to SnO<sub>2</sub> and Fe<sub>2</sub>O<sub>3</sub> were observed matching well with standard JCPDS card no- 721147 of cassiterite SnO<sub>2</sub> and 79-1741 of corundum hematite. The same peaks were also identified in the composite sample for both the compounds. Absence of any other impurity or phase in the composite indicated no other phase is formed in composite material. Low concentration of Fe<sub>2</sub>O<sub>3</sub> in composite material might be

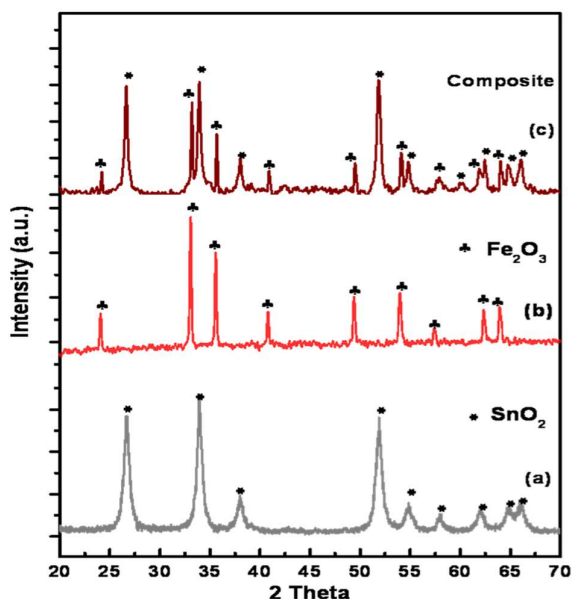


Figure 1: XRD spectra of a) Tin Oxide b) Hematite c) Tin Oxide-Hematite Composite

responsible for its reduced intensity compared to tin oxide. The average crystallite size of  $\text{SnO}_2$  for pure and composite samples was calculated with XRD peak (101) using Debye-Scherrer's equation  $D = k\lambda/\beta_{hkl}\cos\theta$ . The average crystallite size for pure tin oxide was calculated to be 42.94 nm while for composite it reduced to 20.56 nm. Pure tin oxide showed the crystal growth along (101) plane which indicated its reduced state due to the presence of some inherent defects [14]. However, in composite the preferred growth plane reoriented along (211) plane. XRD peaks of  $\text{SnO}_2$  in composite got relatively broadened

compared to individual pure phase  $\text{SnO}_2$  and  $\text{Fe}_2\text{O}_3$ . This might be due to the inhibition of crystallite growth in composite sample induced from diffusion of some Fe atoms in  $\text{SnO}_2$  lattice sites. The similar observations have been already reported in literature for Sb doped  $\text{SnO}_2$  and Fe doped  $\text{SnO}_2$  (7,15,16). This might be due to limit the exposure of high energy surface of (211) plane in the composite [17]. Dominant exposed high energy surface (211) plane interacts strongly with polar water molecule [7]. Lower crystallinity of  $\text{SnO}_2$ - $\text{Fe}_2\text{O}_3$  nano-composite is also supposed to enhance the effective surface area hence the water sensitivity.

To get deep insight of the micro-structural disorders in the  $\text{SnO}_2$ - $\text{Fe}_2\text{O}_3$  composite Raman spectroscopy of the sample was performed (Figure 2a). Characteristic Raman bands of  $\text{SnO}_2$  were observed at around 481, 629 and 770  $\text{cm}^{-1}$  confirming the tetragonal rutile structure of tin oxide. A strong mode near 571  $\text{cm}^{-1}$  is assigned to the in-plane oxygen vacancies in the composite [18]. The two peaks observed for tin oxide at 546 and near 693  $\text{cm}^{-1}$  are closely related to the crystal vacant sites and micro-structural disorders [19]. The appearance of IR active mode  $A_{2u}$  near 695  $\text{cm}^{-1}$  can be assigned to the decreased crystallite growth and hence increased grain boundary defects. The band near 546  $\text{cm}^{-1}$  is known to arise due to the imperfections or distorted symmetry of the particle surface. The signature

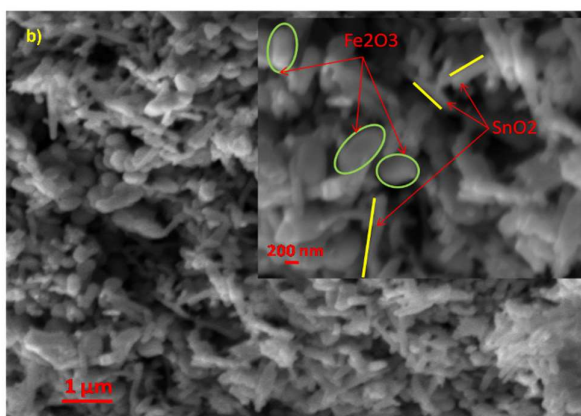
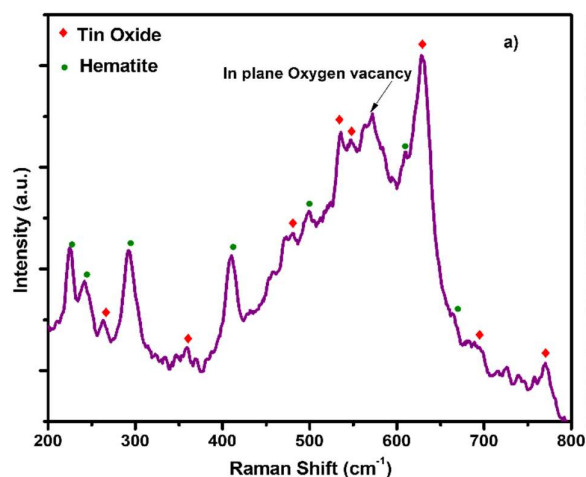


Figure 2: (a) Raman spectrum and (b) SEM image of the synthesized composite

bands for hematite at 226, 243, 293 and 411  $\text{cm}^{-1}$  correspond to the corundum crystal structure. The band between 200-300  $\text{cm}^{-1}$  are assigned to the vibration modes related to iron atoms while at higher frequency region (400-650  $\text{cm}^{-1}$ ) modes are ascribed to vibration of oxygen atoms [13]. The Raman forbidden mode at wave number 660  $\text{cm}^{-1}$  is assigned to the presence of structural disorder in hematite (20). Raman results are in agreement with the XRD that the composite synthesized from  $\text{SnO}_2$  and  $\text{Fe}_2\text{O}_3$  have reduced crystallite size and more structural defects than the parent compounds.

Figure 2(b) represents the SEM image of the synthesized composite. The inset represents the high resolution SEM image of the composite. Two distinct morphologies of the particles can be clearly seen. The EDAX spectra revealed the rod and oval shaped particles are  $\text{SnO}_2$  and  $\text{Fe}_2\text{O}_3$  respectively (figure 3 a & b). The oval shaped hematite particles were seen in close contact with tin oxide nano rods as evident from SEM. Both type of oxide particles showed a broad range of size distribution. The average grain size for  $\text{Fe}_2\text{O}_3$  particles was estimated to be 350 nm. Nano rods with a thickness of 200 nm and length up to 1.2  $\mu$  could be resolved by high resolution SEM image. Tin oxide particles were found accumulated with each other, may be due to reduce the exposure of high energy surface (211) and minimize the surface energy as inferred from the XRD data. The oval shaped hematite particles are attached to the tin

oxide rods in close contact. Wide spread distribution of varying size pores can be seen throughout the composite. The rod shaped morphology of the tin oxide particles increased the effective surface area of the composite, making it more reactive towards the adsorption and dissociation of large number of water molecules.

To investigate the energy levels created in the forbidden energy region due to the defects like anion, cation vacancies or interstitials, room temperature photoluminescence spectroscopy of the pure and composite samples was performed (Figure 4). To ensure the emission from the trap states like self trapped excitons, vacancies and interstitials the excitation was done using a 375 nm laser source. Two major emissive regions were observed in PL spectra near 500 and 560 nm. Both the spectra showed a peak near 430 nm which can be ascribed to metal interstitials or dangling bonds [21, 16]. However, in case of composite this peak has become broad which indicates the presence of other defects also which are obvious. When the size of the crystallite reduces it introduces many other structural defects. The peak at 500 nm is originated from the deep trap emission and is assigned recombination from conduction band to the sub bridging oxygen or in-plane vacancies. This peak has become quenched in the  $\text{SnO}_2$ - $\text{Fe}_2\text{O}_3$  composite due to the presence of  $\text{Fe}_2\text{O}_3$ . As  $\text{Fe}_2\text{O}_3$  is present in

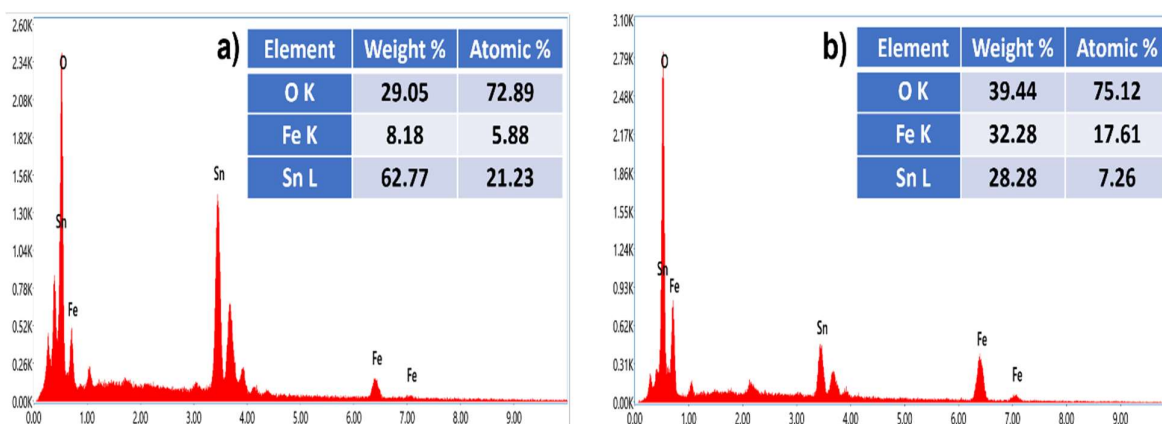


Figure 3: (a) Spot EDAX rod shaped particles (b) Spot EDAX oval shaped particles

large concentrations a process known as cross relaxation can lead to non-radiative energy

Vibrational modes observed at 1245, 1121, 1055 and 995  $\text{cm}^{-1}$  are ascribed to the Sn-OH

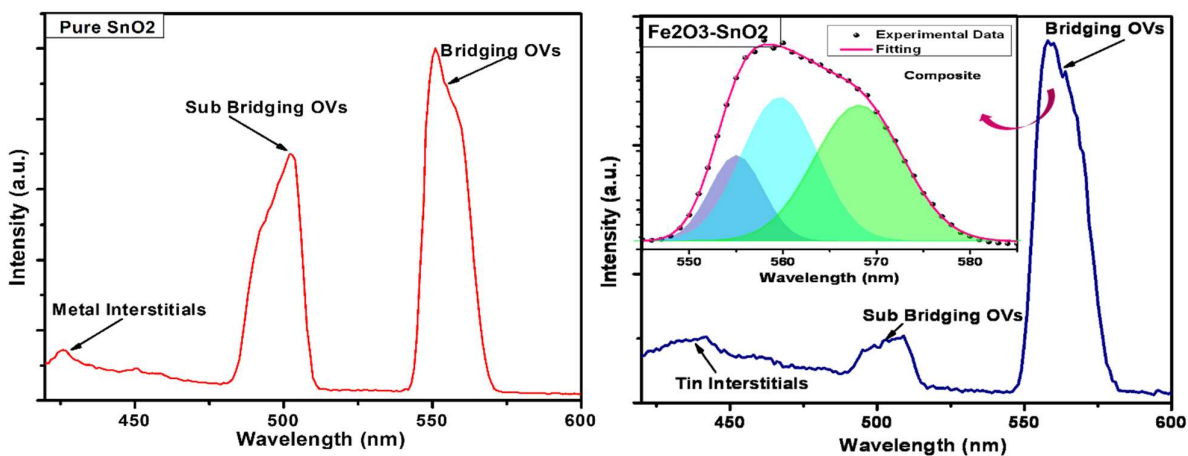


Figure 4: Photoluminescence spectra of Pure SnO<sub>2</sub> and SnO<sub>2</sub>-Fe<sub>2</sub>O<sub>3</sub> Composite

exchange between two neighbouring Fe<sup>3+</sup> centers that quenches the radiative process [22,23]. The other major peak at 560 nm is assigned to the bridging oxygen vacancy. In the composite the peak was found slightly broadened. To get more insight into the origin of peak, it was deconvoluted by multi peak Gaussian fitting into three peaks centered at 555, 559.68 and 568 nm. The emission in this green region is assigned to the recombination of electron from neutral oxygen vacancy center with the singly or doubly ionized oxygen vacancy centers located deep in the energy gap [24]. Furthermore, a valence band edge transition (band gap  $\sim 2.0$  eV) is supposed to contribute to the peak centered at 568 nm [8]. FTIR spectroscopy of the composite sample was performed in the range 4000-400  $\text{cm}^{-1}$  to investigate the interaction of water molecules on its surface. Figure 5 represents the FTIR spectra of composite sample treated with water and finally dried at 50 °C. Vibrational modes observed at 477 and 539  $\text{cm}^{-1}$  are characteristic of the lattice vibrations of hematite related to Fe-O stretching [25] Vibrational mode at 619  $\text{cm}^{-1}$  is assigned to the Sn-O stretching in SnO<sub>2</sub> crystal lattice. Vibrational modes at 1622 and around 3150 are attributed to H-O-H bond bending and stretching respectively due to physisorbed water molecules on sample surface [26].

bond stretching vibrations generated due to the chemi-dissociation of water molecules on the under coordinated composite surface at terminal sites. A sharp band at 1400  $\text{cm}^{-1}$  is assigned to the Sn-O-Sn bridge vibration harmonics on the sample surface formed after

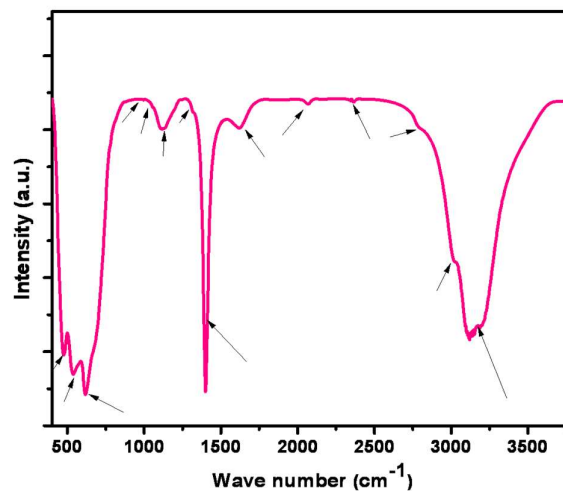


Figure 5: FT-IR Spectra of water treated SnO<sub>2</sub>-Fe<sub>2</sub>O<sub>3</sub> composite

the heating of wet sample [27]. A weak band near 3020  $\text{cm}^{-1}$  is due to the Sn-OH stretching of bridging hydroxyl groups while the broad band centered at 3140  $\text{cm}^{-1}$  contains several modes which may be assigned to the different stretching modes of -OH group existing in different forms and environment like Sn-OH

(Bridging), H<sub>2</sub>O- hydrogen bonded to surface hydroxyl etc. indicating highly active composite surface. The weak bands between 2050 to 2800 cm<sup>-1</sup> are assigned to various symmetric and coupled vibrations of water molecules [28].

give rise to ionic conduction within the cell. Dry composite based cell also showed a diffusion tail which may be due to the presence of some dissociated water molecules already present at the electrode interface owing to composite's strong affinity towards water,

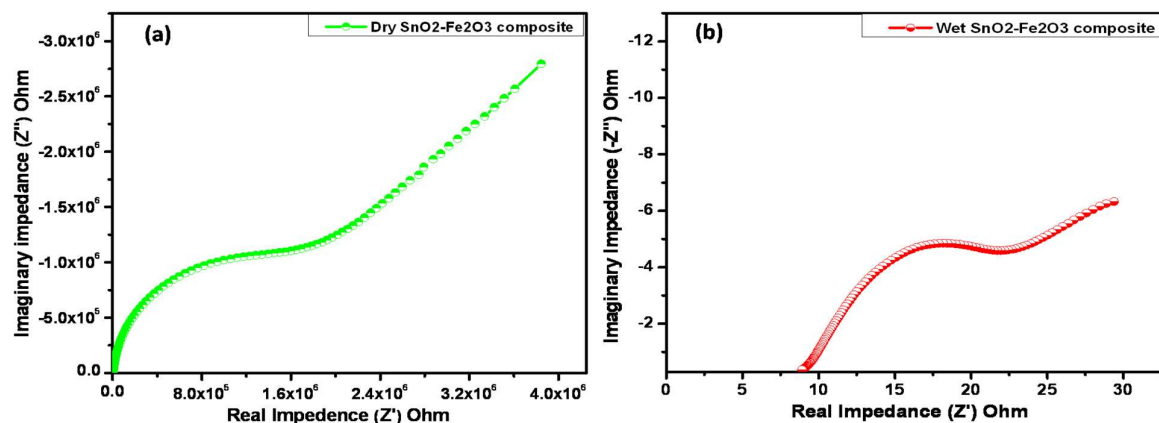


Figure 6: EIS Spectra of (a) dry and (b) wet composite based hydroelectric cell

Dissociation of water molecules and the ionic conduction within the composite based cell was further confirmed by electrochemical impedance spectroscopy. The EIS spectra of dry and wet composite based hydroelectric cell is presented in figure 6(a) and 6(b) respectively. In both the spectra a semicircle is followed by a diffusion tail at low frequency. Plot indicating the cell spectra in dry state (Figure 6a) exhibited a high resistance of the order of mega ohm. After the cell was partially dipped in the de-ionized water, the drop in cell resistance was observed of the order of 10<sup>5</sup> (Figure 6b). This is due to the reason that as the water falls on to the cell it dissociatively adsorbed on the pellet surface and forms a chemisorbed layer of -OH groups which is also verified by FTIR results. The physisorption of water molecules take place on the chemisorbed hydroxyl layer due the electrostatic field created by this layer on the material surface. Proton hopping starts on physisorbed water layer by Grotthuss mechanism. The hopping protons get trapped inside the nanopores, creates electric field of the order of 10<sup>4</sup> V/cm that is high enough to dissociate physisorbed water molecules [1]. The dissociated ions migrate towards the respective electrodes and

adsorbed from the humid environment.

In order to investigate the effect of hematite on the polarization losses in SnO<sub>2</sub>-Fe<sub>2</sub>O<sub>3</sub> composite based hydroelectric cell the V-I curves were plotted shown in Fig 7 (a, b). In the figure 7 (a) and (b), region AB represents the activation losses at low current density region where point A indicates the open circuit potential of the cell. BC represents the ohmic loss region where the potential falls due to the resistance of the material faced by the migrating ions. Region CD represents the mass transport loss in the cell at high current density. The composite based cell delivered short circuit current of I<sub>sc</sub> ~28.3 mA and OCP ~0.95 V while bare SnO<sub>2</sub> based cell delivered I<sub>sc</sub> ~22.2 mA and OCP ~ 0.797 V. The maximum power output for composite based HEC increased to 6.1 mW/cm<sup>2</sup> from 4.0 mW/cm<sup>2</sup> for bare SnO<sub>2</sub> based HEC. A high OCP was observed in composite base cell in comparison to the SnO<sub>2</sub> based HEC.

It may be due the internal conversion of Sn<sup>2+</sup> to Sn<sup>4+</sup> in pure SnO<sub>2</sub>, which onsets a negative redox at cathode and lowers the overall cell potential. The same effect was also observed in magnetite based HEC (6). A high activation loss of 0.34 V was observed for bare SnO<sub>2</sub>

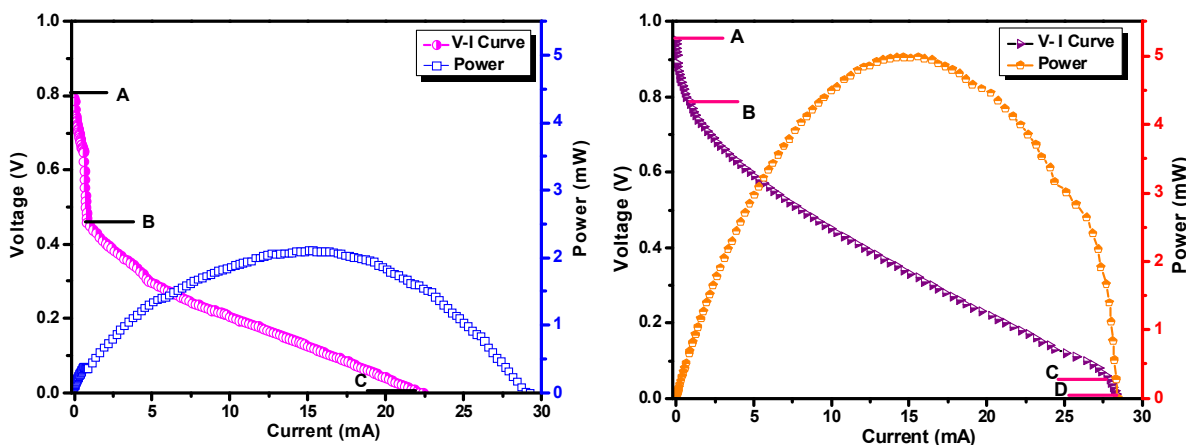


Figure 7: V-I polarisation curves of HEC (a) Bare SnO<sub>2</sub> (b) SnO<sub>2</sub>-Fe<sub>2</sub>O<sub>3</sub> composite

based HEC, however in the composite based cell the activation loss reduced to 0.15 V. In general SnO<sub>2</sub> based hydroelectric cell shows high activation loss in spite of inherent defects. One of the causes of this activation loss is the high bonding energy of hydrogen to SnO<sub>2</sub> surface at high pH which limits the hydrogen evolution from cathode surface [2]. In contrast to bare SnO<sub>2</sub> the OCP and I<sub>sc</sub> were found to be increased in composite based cell along with reduced activation loss. It may be possible that Fe<sup>3+</sup> cations substituted Sn<sup>2+</sup> in the composite and therefore eliminated the Sn<sup>2+</sup>/Sn<sup>4+</sup> redox reaction within the material, which is verified by the observed high OCP in composite based HEC. Further, as long as the tin oxide surface has Sn<sup>2+</sup> sites, it facilitate the evolution of hydrogen gas however, oxidation of Sn<sup>2+</sup> to Sn<sup>4+</sup> surface causes the surface rearrangement and makes it sluggish for hydrogen evolution reaction which may contribute to high activation barrier in pure SnO<sub>2</sub> based cell [29]. It may be possible that the substitution of Sn<sup>2+</sup> by Fe<sup>3+</sup> formed Fe<sup>3+</sup>-V<sup>0</sup> defect pairs reduced the conversion of Sn<sup>2+</sup> to Sn<sup>4+</sup>, releases hydrogen easily, which ultimately reduced the activation barrier in composite based hydroelectric cell. The ohmic region represents the resistance faced by the charge flow due to the internal resistance of the cell. This region also represents the useful window where the cell operates. A linear ohmic region was observed in composite based cell due low internal resistance of the cell. It improved easy charge migration within the material. Region

CD represents the mass transport losses. This loss was almost negligible in tin oxide based cell however a prominent mass transfer loss was observed in composite based cell compared to tin oxide. It may be due the increased crowding of ions at electrode due to more number of dissociated ions and their effective transfer to the electrode interface [7].

**4. Conclusions:** A tin oxide-hematite composite was synthesized for green energy generation by hydroelectric cell. The composite based cell delivered short circuit current of I<sub>sc</sub> ~28.3 mA and OCP ~0.95 V while bare SnO<sub>2</sub> based cell delivered I<sub>sc</sub> ~22.2 mA and OCP ~0.797 V. Tin oxide based cells shows high activation losses due to the inherent defects and therefore presence of Sn<sup>2+</sup> sites on the surface. The oxidation of Sn<sup>2+</sup> to Sn<sup>4+</sup> increased the internal losses in the cell EMF and found responsible for sluggish cathode kinetics. Composite of tin oxide with hematite increased the effective surface area with water interaction thus increased current output in composite based cell. It also reduced the internal losses by replacing Sn<sup>2+</sup> by Fe<sup>3+</sup> cations in the lattice. Incorporation of Fe<sup>3+</sup> cation in SnO<sub>2</sub> lattice improved the cathode kinetics for hydrogen evolution and hence reduced the activation energy barrier at the electrode material interface. Hence SnO<sub>2</sub>-Fe<sub>2</sub>O<sub>3</sub> composite based cell is a promising solution to deliver high power density with reduced cost compared to tin oxide based hydroelectric cell. Further engineering of the

composite can enhance the power generation which can be explored in future.

**Acknowledgements:** Authors are thankful to the Director, CSIR-National Physical Laboratory Delhi, for the support to carry out the research work.

## 5. References:

- [1] R. K. Kotnala and J. Shah, Green hydroelectrical energy source based on water dissociation by nanoporous ferrite, *Int. J. Energy Res*, 40, **2016**, 1652–61.
- [2] J. Shah, S. Jain, A. Shukla, R. Gupta, R. K. Kotnala, A facile non-photocatalytic technique for hydrogen gas production by hydroelectric cell, *42(52)*, **2017**, 30584-90
- [3] R. K. Kotnala, Rekha Gupta, Abha Shukla, Shipra Jain, Anurag Gaur, and Jyoti Shah, Metal Oxide Based Hydroelectric Cell for Electricity Generation by Water Molecule Dissociation without Electrolyte/Acid, *J. Phys. Chem. C*, 122, **2018**, 18841–49.
- [4] R. Das, J. Shah, S. Sharma, P. B. Sharma, R. K. Kotnala, Electricity generation by splitting of water from hydroelectric cell: An alternative to solar cell and fuel cell, *Int J Energy Res.*, **2020**, 1–24.
- [5] R. K. Kotnala, R. Das, J. Shah, S. Sharma, C. Sharma, P. B. Sharma, Red mud industrial waste translated into green electricity production by innovating an ingenious process based on Hydroelectric Cell, *Journal of Environmental Chemical Engineering*, 10, **2022**, 107299.
- [6] S. Jain, J. Shah, S. R. Dhakate, G. Gupta, C. Sharma, and R. K. Kotnala, Environment-Friendly Mesoporous Magnetite Nanoparticles-Based Hydroelectric Cell, *J. Phys. Chem. C*, 122 (11), **2018**, 5908–16.
- [7] J. Shah, A. Shukla, and R. K. Kotnala, Highly Accelerated, Sustainable, Abundant Water Splitting at Room Temperature Generating Green Electricity by Sb-Doped SnO<sub>2</sub> Hydroelectric Cell, *ACS Sustainable Chem. Eng.*, 9, **2021**, 15229–38.
- [8] D. Yan, W. Chen, Y. Zou, R. Chen, S. Zang, Y. Wang, X. Yao, S. Wang, Insight into the design of defect electrocatalysts: From electronic structure to adsorption energy, *materials today*, 31, **2019**, 7-68.
- [9] Y. Sun, A. J. Darling, Y. Li, K. Fujisawa, C. F. Holder, H. Liu, M. J. Janik, M. Terrones and R. E. Schaak, Defect-mediated selective hydrogenation of nitroarenes on nanostructured WS<sub>2</sub>, *Chem. Sci.*, 10, **2019**, 10310-17.
- [10] Y. Sun, L. Chen, Y. Bao, Y. Zhang, J. Wang, M. Fu, J. Wu, D. Ye, The Applications of Morphology Controlled ZnO in Catalysis, *Catalysts*, 6, **2016**, 188.
- [11] B. Meyer, D. Marx, O. Dulub, U. Diebold, M. Kunat, D. Langenberg and C. Wöll, Partial Dissociation of Water Leads to Stable Superstructures on the Surface of Zinc Oxide. *Angewandte Chemie International Edition*, 43, **2004**, 6641-45.
- [12] J. Shah, S. Jain, B. Gahtori, C. Sharma and R. K. Kotnala, Water Splitting on the Mesoporous Surface and Oxygen Vacancies of Iron Oxide Generates Electricity by Hydroelectric Cell, *Materials Chemistry and Physics*, 258, **2021**, 123981.
- [13] S. Jain, J. Shah, N. S. Negi, C. Sharma, R. K. Kotnala, Significance of interface barrier at electrode of hematite hydroelectric cell for generating ecopower by water splitting, *Int J Energy Res.*, **2019**, 1–13.
- [14] M. Batzill and U. Diebold, The surface and materials science of tin oxide, *Prog. Surf. Sci.*, 79, **2005**, 47–154.
- [15] M. V. Vaishampayan, R. G. Deshmukh, P. Walke, I. S. Mulla, Fe-doped SnO<sub>2</sub> nanomaterial: A low temperature hydrogen sulfide gas sensor, *Materials Chemistry and Physics*, 109, **2008**, 230–34.
- [16] S. Rania, S. C. Royb, N. Kararc and M.C. Bhatnagar, Structure, microstructure and photoluminescence properties of Fe doped SnO<sub>2</sub> thin films, *Solid State Communications*, 141, **2007**, 214–18.
- [17] F. Mueller, D. Bresser, V. S. K. Chakravadhanula, S. Passerini, Fe-doped SnO<sub>2</sub> nanoparticles as new high capacity anode material for secondary lithium-ion batteries, *Journal of Power Sources*, 299, **2015**, 398-402.
- [18] L. Z. Liu, X. L. Wu, F. Gao, J. C. Shen, T. H. Li, P. K. Chu, Determination of surface oxygen vacancy position in SnO<sub>2</sub> nanocrystals

- by Raman spectroscopy, *Solid State Commun.*, 151, **2011**, 811.
- [19] P. Sangeetha, V. Sasirekhab and V. Ramakrishnan, Micro-Raman investigation of tin dioxide nanostructured material based on annealing effect, *J. Raman Spectrosc.* 42, **2011**, 1634–39.
- [20] A. M. Jubb and H. C. Allen, Vibrational Spectroscopic Characterization of Hematite, Maghemite, and Magnetite Thin Films Produced by Vapor Deposition, *Applied energy materials & Interfaces*, 2 (10), **2010**, 2804–12.
- [21] D. Calestani, L. Lazzarini, G. Salviati, and M. Zha, Morphological, structural and optical study of quasi-1D SnO<sub>2</sub> nanowires and nanobelts, *Cryst. Res. Technol.*, 40(10–11), **2005**, 937 – 941.
- [22] R. K. Mishra, A. Kushwaha and P. P. Sahay, Influence of Cu doping on the structural, photoluminescence and formaldehyde sensing properties of SnO<sub>2</sub> nanoparticles, *RSC Adv.*, 4, **2014**, 3904.
- [23] B. Morais, P. J. S. Foot, R. A. Kresinski, Synthesis and photoluminescent properties of Sm<sup>3+</sup>-doped SnO<sub>2</sub> nanoparticles. *Ceramics International.*, 42 (16), **2016**.
- [24] V. Kumar, H C Swart, M. Gohain, B. C B Bezuidenhoudt, A. J. Vuuren, M. Lee and O. M. Ntwaeaborwa, The role of neutral and ionized oxygen defects in the emission of tin oxide nanocrystals for near white light application, *Nanotechnology*, 26, **2015**, 295703.
- [25] U. R. Arilasita, Suharno, H. Widiyandari, and B. Purnama, Effect of Synthesis Temperature on Structural and Magnetic Properties in Hematite ( $\alpha$ -Fe<sub>2</sub>O<sub>3</sub>) Nanoparticles Produced by Co-Precipitation Method, *Defect and Diffusion Forum*, 417, **2022**, 219-25.
- [26] E. W. Thornton. P.G. Harrison, Surface Hydroxyl Groups and the Chemisorption of Carbon Dioxide and Carbon Monoxide on Tin (IV) Oxide, *Chem. Soc., Faraday Trans. 1*, **71**, **1975**, 461-72.
- [27] D. Amalric-Popescu, F. Bozon-Verduraz, Infrared studies on SnO<sub>2</sub> and Pd/SnO<sub>2</sub>, *Catalysis Today*, 70, **2001**, 139–54.
- [28] B. L. Mojet, S. D. Ebbesen and Leon Lefferts, Light at the Interface: The Potential of Attenuated Total Reflection Infrared Spectroscopy for Understanding Heterogeneous Catalysis in Water, *Chemical Society Reviews*, 39(12), **2010**, 4643-55.
- [29] C. Salvini, M. R. Fiorentin, F. Risplendi, F. Raffone, and G. Cicero, Active Surface Structure of SnO<sub>2</sub> Catalysts for CO<sub>2</sub> Reduction Revealed by Ab Initio Simulations, *J. Phys. Chem. C*, 126 (34), **2022**, 14441–47.